



RESEARCH ARTICLE

10.1029/2020JA028800

Electron Bulk Heating at Saturn's Magnetopause

I. Cheng¹ , N. Achilleos¹ , A. Masters² , G. Lewis¹, M. Kane³ , and P. Guio^{1,4} 

Key Points:

- Electron bulk heating at Saturn's magnetopause is used to test hypotheses about magnetic reconnection
- Observations suggestive of locally open magnetopause tend to exhibit electron heating closer to the theoretical prediction for reconnection
- $\Delta\beta$ magnetic shear parameter space discriminates well between events with evidence of energization and those without

Correspondence to:

I. Cheng,
i.cheng.19@ucl.ac.uk

Citation:

Cheng, I., Achilleos, N., Masters, A., Lewis, G., Kane, M., & Guio, P. (2021). Electron bulk heating at Saturn's magnetopause. *Journal of Geophysical Research: Space Physics*, *126*, e2020JA028800. <https://doi.org/10.1029/2020JA028800>

Received 8 OCT 2020
Accepted 10 MAR 2021

¹Department of Physics and Astronomy, University College London, London, UK, ²Blackett Laboratory, Imperial College London, London, UK, ³Harford Research Institute, Bel Air, MD, USA, ⁴Department of Physics and Technology, Arctic University of Norway, Tromsø, Norway

Abstract Magnetic reconnection at the magnetopause (MP) energizes ambient plasma via the release of magnetic energy and produces an “open” magnetosphere allowing solar wind particles to directly enter the system. At Saturn, the nature of MP reconnection remains unclear. The current study examines electron bulk heating at MP crossings, in order to probe the relationship between observed and predicted reconnection heating proposed by Phan et al. (2013, <https://doi.org/10.1002/grl.50917>) under open and closed MP, and how this may pertain to the position of the crossings in the $\Delta\beta$ -magnetic shear parameter space. The electron heating for 70 MP crossings made by the Cassini spacecraft from April 2005 to July 2007 was found using 1d and 3d moment methods. Minimum variance analysis was used on the magnetic field data to help indicate whether the MP is open or closed. We found better agreement between observed and predicted heating for events suggestive of locally “open” MP. For events suggestive of locally “closed” MP, we observed a cluster of points consistent with no electron heating, but also numerous cases with significant heating. Examining the events in the $\Delta\beta$ -magnetic shear parameter space, we find 83% of events without evidence of energization were situated in the “reconnection suppressed” regime, whilst between 43% to 68% of events with energization lie in the “reconnection possible” regime depending on the threshold used. The discrepancies could be explained by a combination of spatial and temporal variability which makes it possible to observe heated electrons with different conditions from the putative reconnection site.

Plain Language Summary Saturn's magnetic cavity in space is marked by a boundary called the magnetopause. Particles from the Sun can enter this region via a process called magnetic reconnection. However, the conditions under which this process can occur on the boundary remains unclear. We used the heating of electrons detected by the Cassini spacecraft during crossings of this boundary to study the effects of different conditions on the viability of reconnection at Saturn's magnetopause. We found that most of the crossings which showed evidence of significant electron heating close to theoretical predictions were also at locations where the magnetopause was open (i.e., locations where solar particles can enter Saturn's territory) and/or where the local conditions were suitable for reconnection to take place.

1. Introduction

The magnetopause (MP) is the natural boundary of a planetary magnetosphere. It is formed by the interaction between the solar wind and planetary magnetosphere. At Saturn, it separates the magnetospheric magnetic field and plasma (mainly from the moon Enceladus) from the interplanetary magnetic field (IMF) and solar wind plasma that has to flow around the magnetospheric obstacle (Baines et al., 2018). Cassini observations of magnetic field and plasma have also revealed that the disk-like magnetosphere imposes an “inflation” of the magnetopause at near-equatorial latitudes (Pilkington et al., 2014).

Magnetic reconnection is an important process at this boundary as it can energize plasma via the release of magnetic energy when the fields undergo a topological change to a lower energy state (Øieroset et al., 2001). The signature of this process is heated high speed plasma jets (Yamada et al., 2010). Direct evidence of magnetic reconnection signatures has been observed at Saturn's magnetopause. For example, McAndrews et al. (2008) reported two magnetopause crossings with heating in the electrons and ions along field lines just outside the magnetopause that is highly suggestive of energization comparable to that associated with the reconnection process at Earth.

© 2021. The Authors.
This is an open access article under the terms of the [Creative Commons Attribution License](https://creativecommons.org/licenses/by/4.0/), which permits use, distribution and reproduction in any medium, provided the original work is properly cited.

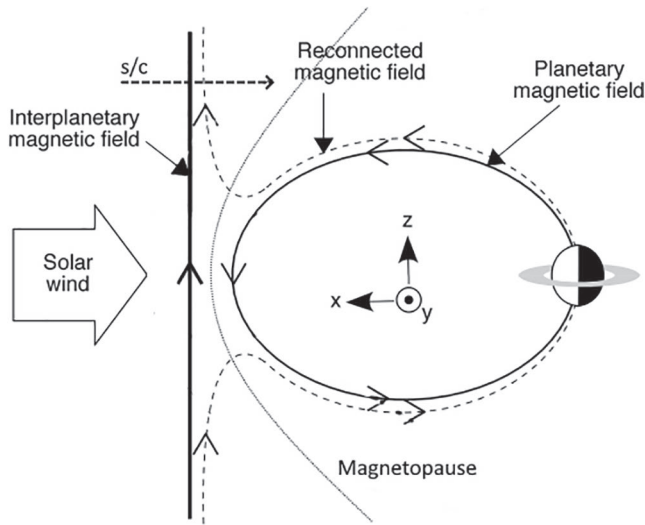


Figure 1. Schematic illustrating day side magnetic reconnection at Saturn's magnetopause (dotted line) under northward IMF. The reconnected (open) magnetic field line is shown as dashed line. Adapted from Masters et al. (2012). IMF, interplanetary magnetic field.

In the absence of magnetic reconnection, the magnetosphere would be closed and thus have no magnetic connection with the solar wind. The planetary magnetic field lines form closed loops connecting one pole to the other (Figure 1). In this closed configuration, the normal field component (i.e., the direction perpendicular to the local MP surface, also the minimum variance direction for the magnetic field) is zero. However, under the right conditions, the IMF embedded in the solar wind can reconnect with the planetary field. This leads to an open magnetosphere with magnetic connection across the MP current layer where solar wind plasma can directly enter the magnetosphere. Locally, the normal component of the magnetic field relative to the MP surface becomes non-zero. This is illustrated in Figure 1. The solar wind can couple with the magnetosphere via "large scale" reconnection and/or "viscous" interaction like Kelvin-Helmholtz instabilities; the latter of which has been suggested as the dominant mode at Saturn (Masters, 2018).

The question that arises is: Under what conditions is reconnection viable at Saturn's magnetopause? Swisdak, et al. (2003) hypothesized that viable reconnection under a large difference in plasma β (ratio of plasma to magnetic pressure) across the MP also requires a high magnetic shear. Masters et al. (2012) analyzed 70 magnetopause crossing events at Saturn detected by the Cassini spacecraft and showed that the plasma β is higher in Saturn's magnetosheath (typically equal to 10) than in Earth's. This is

believed to restrict reconnection to regions on the magnetopause with almost anti-parallel magnetic fields either side. Reconnection is suppressed when the following condition is satisfied:

$$|\Delta\beta| > \frac{2L}{d_i} \tan\left(\frac{\theta}{2}\right) \quad (1)$$

where L is the current layer thickness, d_i is the ion inertial length, and θ is the magnetic shear angle across the current layer. This is the general diamagnetic suppression condition, introduced by Swisdak et al. (2010) and tested by Phan et al. (2010) using evidence from solar wind observations. Essentially, the theory suggests that a higher $|\Delta\beta|$ across the current layer is less favorable for reconnection as the associated diamagnetic drift of charged particles can disrupt the reconnection jets.

In this study, we use bulk electron heating (i.e., the scalar temperature change) at MP crossings ("events") as a possible reconnection signature to test the following hypotheses. (1) Events where the MP boundary is locally closed would have essentially no observed electron temperature change (ΔT_e) in the magnetosheath boundary layer (MSBL), whereas most events with locally open boundary should have observed change close to the theoretical prediction. (2) Events with evidence of plasma heating should generally be in the "reconnection possible" regime, whereas those without such evidence should lie in the "reconnection suppressed" regime in the $|\Delta\beta|$ -magnetic shear parameter space. This investigation examines the crossings from Masters et al. (2012) in more detail, in order to probe the relationship between observed and predicted ΔT_e , and how this may pertain to the position of the crossings in the $|\Delta\beta|$ -magnetic shear parameter space.

2. Cassini Data Set

The data set consists of 70 magnetopause (MP) crossings made by the Cassini spacecraft from April 2005 to July 2007, previously reported by Masters et al. (2012). These 70 events have full plasma β measurements including thermal H^+ and H_2^+ / He^{++} pressures on both sides of the MP and can be found in the original database in Masters et al. (2012).

For this study, magnetic field and particle data were used to further characterize the MP crossings. These measurements were obtained by the following two instruments on-board Cassini: The dual-technique magnetometer (MAG) (Dougherty et al., 2004), and the electron spectrometer (ELS) part of the Cassini Plasma Spectrometer (CAPS) instrument (Young et al., 2004). MAG provides the magnetic field measurements and

1-min averaged data were used along with Kronocentric solar magnetospheric (KSM) coordinates, where X points from center of Saturn to the Sun, Y points in the direction $\Omega \times X$ (where Ω is Saturn's rotational/magnetic dipole axis), and Z completes the right-handed coordinate system. Moments derived from 8-s averaged distributions in the ELS data provide electron density and temperature. The ELS instrument has eight anodes which sweeps through 63 bins covering an energy range of 0.6 eV–28.25 keV in 2 s. The ELS is able to detect electron density as low as $\sim 10^3 \text{ m}^{-3}$ (Young et al., 2005). The field of view of each anode is $20^\circ \times 5^\circ$ (thus $160^\circ \times 5^\circ$ for all eight anodes). An actuator sweeps the anodes back and forth covering $\sim 2\pi$ sr of solid angle. The coverage may be increased if the spacecraft is rolling. For this study, we used anode 5 for all electron measurements as it has relatively large pitch angle coverage (relative to the local magnetic field) throughout an actuation cycle, compared to other anodes.

The MAG data were obtained from The Planetary Plasma Interactions (PPI) Node of the Planetary Data System (PDS). The ELS and moments data were obtained from the MSSL (Mullard Space Science Laboratory) server.

3. Methods

In this section, we describe our methodology used in the statistical survey to evaluate the amount of bulk heating of magnetosheath electrons entering into the magnetopause current layer (MPCL). We compare the observed heating (ΔT_e) to the theoretical bulk heating due to reconnection based on inflow conditions (Phan et al., 2013), in an attempt to determine whether the observed heating was potentially caused by magnetic reconnection at Saturn's magnetopause. Crucially, note that the theoretical value of ΔT_e derived from the data assumes that the observations are a faithful representation of the conditions at the reconnection site. This is not necessarily the case; we discuss this point further, later in the study.

The crossing times and intervals of the 70 MP crossings previously reported by Masters et al. (2012) were modified on a case by case basis for the purpose of this study. The intervals were identified based on magnetic field rotation from the magnetosheath configuration (usually weaker field) to the magnetosphere configuration (usually stronger field) in conjunction with the electron moments showing signatures of transition from magnetosheath (high density, low temperature) to magnetosphere (low density, high temperature). The full plasma β measurements on both sides of the MPCL were from the original database in Masters et al. (2012), while all other parameters were determined in this study.

For each event, the heating of magnetosheath electrons was calculated by subtracting the average temperature in the pristine magnetosheath from that of the magnetosheath edge of the magnetopause (“exhaust”), that is, $\Delta T_{\text{obs}} = T_{\text{exh}} - T_{\text{sh}}$. The pristine magnetosheath was defined by an interval outside the MP interval where the plasma moments and magnetic field were relatively stable, typically spanning 1–2 min (see Figure 4 for example). To achieve this, we required two pieces of information: (1) A way to identify the “inner edge” of the exhaust region. (2) A reliable way of calculating the temperature of the magnetosheath electrons in each region.

To address the first requirement, Phan et al. (2013) used the “high-energy tail” of an electron energy spectrum as a means of detecting the first appearance of the magnetospheric electron population and thus where the magnetosheath boundary layer (MSBL) “stops.” This is the “inner edge” of the exhaust, beyond which the magnetospheric population dominates. If the temperature in the MSBL is significantly greater than that of the pristine magnetosheath, then it is said to be a heated magnetosheath population. To determine if this heating is related to reconnection, we need to know whether the spacecraft is in an exhaust signaled by enhanced velocity measurements (“jets”) compared to the ambient plasma. However, bulk electron and ion velocity data are not available for most events as CAPS does not normally view the entire 4π steradians of solid angle due to three-axis stabilization (stare mode). Valid measurements of the plasma bulk velocity can only be obtained when the bulk flow is in the field-of-view of CAPS (Arridge et al., 2009; Thomsen et al., 2010). The INCA sensor measurements on the MIMI instrument of Cassini were successfully used to derive O^+ plasma flow speeds in Saturn's magnetosphere (Kane et al., 2020). However, this method requires relatively stable conditions for usually 30 min; as such, boundaries where conditions tend to be more variable were avoided. Based on this limitation, we proceeded with determining the inner edge of the exhaust as above (i.e., Phan et al.'s “tail” method) but in the absence of velocity data. Note that this

inner edge could only be considered the location of an actual reconnection “exhaust” if the ΔT_e supported that hypothesis; otherwise it is the inner edge of a “candidate” exhaust.

To determine magnetosheath T_e , we used two methods: the 3d moment method and the 1d moment method. These methods are well documented in Lewis et al. (2008). For completeness, a summary of the key equations is given below.

The 3d moment method integrates the velocity distribution function $f(\mathbf{v})$ measured by ELS at a given time over the velocity volume. The density (n) and temperature (T) moments are calculated as follows:

$$\begin{aligned} n &= \int f(\mathbf{v}) d^3\mathbf{v} \\ T &= \frac{m}{3nk_B} \int v^2 f(\mathbf{v}) d^3\mathbf{v} \end{aligned} \quad (2)$$

where k_B is the Boltzmann constant and m is the particle mass. The temperature equation uses the average kinetic energy per particle due to thermal motion in three degrees of freedom $m\langle v^2 \rangle / 2 = 3k_B T / 2$ and $\langle v^2 \rangle = 1/n \int v^2 f(\mathbf{v}) d^3\mathbf{v}$, under the assumptions of a Maxwellian distribution and zero bulk flow. Arridge et al. (2009) showed that the bulk kinetic energy is always more than 100 times smaller than the typical peak electron energy (~ 100 eV), thus justifying the zero bulk velocity assumption. For ions, the bulk flow cannot be neglected and $v \rightarrow (\mathbf{v} - \mathbf{v}_b)$ where \mathbf{v}_b is the bulk flow velocity. Under the assumptions of an isotropic $f(\mathbf{v})$ for the electrons ($d^3\mathbf{v} \rightarrow 4\pi v^2 dv$), and a constant $f(\mathbf{v})$ across each energy bin, the integrals in Equation 2 become a sum over 63 energy bins in ELS:

$$\begin{aligned} n &= \frac{4\pi}{3} \sum_{i=1}^{i=63} f(v_{i,m}) (v_i^3 - v_{i-1}^3) \\ T &= \frac{4\pi m}{15nk_B} \sum_{i=1}^{i=63} f(v_{i,m}) (v_i^5 - v_{i-1}^5) \end{aligned} \quad (3)$$

where subscripts $i, i - 1$ represent the upper and lower boundary of the i th energy bin, and $v_{i,m} = \sqrt{2E_{i,m} / m}$ (where $E_{i,m}$ is the centroid energy of each bin ranging from 0.58 eV to 26 keV) (Lewis et al., 2008). Each term of these summations makes a finite contribution to the total density and temperature. However, as the magnetopause boundary is an intermediate region between the magnetosheath and magnetosphere, the plasma in this region is likely a mixed population of magnetosheath and magnetospheric plasmas. We used a cut-off of 150 eV for delineating two electron populations (cold, <150 eV, and hot, >150 eV). This cut-off is ~ 3 times the modal energy of magnetosheath electrons (typically ~ 50 eV, see for example the peak of the energy distribution in Figure 2a). This is high enough to capture the low energy magnetosheath population, but not so high as to include hotter magnetospheric electrons in the plasma. In this study, we determine both the full temperature by summing over all the energy bins and the “cold population” temperature by summing only bins below 150 eV (bin index $i = 30$).

The 1d moment method assumes that the energy distribution function is Maxwellian, given by:

$$f_{\text{Maxwell}}(E) = n \left(\frac{m}{2\pi k_B T} \right)^{3/2} \exp\left(\frac{-E}{k_B T} \right). \quad (4)$$

In the 1d method, a Gaussian of the form

$$g(E) = A_0 \exp\left(\frac{-(E - A_1)^2}{2A_2^2} \right), \quad (5)$$

where A_0, A_1, A_2 are the height, mean value and standard deviation of the Gaussian respectively, is fitted to the electron counts per second data (or count rate R_c) against energy (E) at a given time from the ELS instrument to extract the energy that maximizes the count rate (i.e., where the derivative $dR_c/dE = 0$). The derivative dR_c/dE is obtained by equating the Maxwellian in Equation 4 to the phase space density (PSD) derived from count rate data using Equation 6, and differentiating with respect to energy:

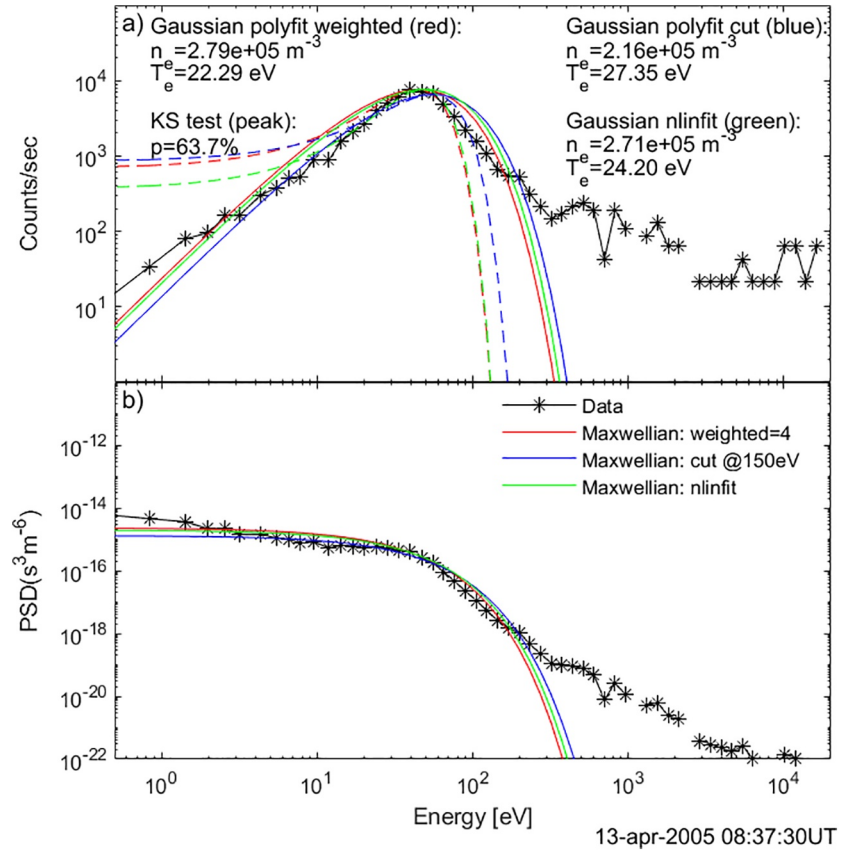


Figure 2. An example of various fitting techniques used in the 1d moment method. The black lines in panel (a and b) are the counts per second data and PSD distribution functions measured by CAPS-ELS on April 13, 2005 at 0837 UT (corrected for photoelectrons). Gaussian curves, fitted using different techniques, shown as dashed lines. Using the density and temperature values derived from the peak of the Gaussian, the corresponding Maxwellian is derived using Equation 4. The Maxwellian curves shown as solid lines are used to perform Kolmogorov-Smirnov (KS) tests against the seven points in the neighborhood of the peak value. The result of this test for the “nlinfit” Maxwellian is shown on the plot.

$$f(v) = \frac{2R_c}{v^4 G(E)}, \quad (6)$$

where $R_c = N/t_a$ is the electron count rate data based on returned electron counts N and accumulation time $t_a = 23.4$ ms; corrected for anode dependent efficiency and then converted to the corrected counts per second, v is the velocity associated with the measurement energy derived from $v = \sqrt{2E/m}$, and $G(E)$ is the instrument energy-dependent geometric factor. By setting $dR_c/dE = 0$, the Maxwellian temperature and density parameters are found by:

$$T = \frac{A_1}{k_B \left(2 + \frac{d \ln G}{d \ln E} \right)} \approx \frac{A_1}{2k_B} \quad (7)$$

$$n = \left(\frac{\pi}{2} \right)^{\frac{3}{2}} \frac{A_0}{G(A_1)} \sqrt{\frac{m}{k_B T}} \exp(2),$$

where A_1 is the estimated peak energy and A_0 is the estimated peak count rate from the Gaussian fit. A corresponding Maxwellian is derived by inserting n and T into Equation 4. We refer the reader to Lewis et al. (2008) for a detailed derivation.

A Kappa distribution (Pierrard & Lazar, 2010) of the following form can also be fitted to the PSD data:

$$f_{\text{kappa}}(v) = \frac{n}{(\pi\kappa w^2)^{\frac{3}{2}}} \frac{(\kappa + 1)}{(\kappa - 1/2)} \left(1 + \frac{v^2}{\kappa w^2}\right)^{-(\kappa+1)}, \quad (8)$$

where $w = \sqrt{(2\kappa - 3)k_B T / \kappa m}$ is the most probable thermal velocity, n is the number density, $\Gamma(x)$ is the Gamma function, κ is the kappa index which determines the slope of the energy spectrum in the high energy tail, and T is the equivalent temperature of the plasma such that $3k_B T/2$ represents the mean energy per particle of the distribution. The full 3d temperature and density moments can be used as plasma parameters in this distribution to fit to observations with a high-energy tail; a low κ value indicates substantive suprathermal tail whilst a high value indicates a distribution close to Maxwellian (i.e., the Maxwellian distribution is a special case of the more general kappa distribution). In the limit $\kappa \rightarrow \infty$, $w = \sqrt{2k_B T / m}$ becomes the most probable speed of a Maxwellian. The kappa index must be larger than the critical value $\kappa_c = 3/2$, where the distribution function collapses and the temperature is not defined.

An example of the fitted curves and corresponding data is shown in Figure 2. Three different routines were used to fit the Gaussian, namely: “polyfit cut,” “polyfit weighted,” and “nlinfit”:

- In “polyfit cut,” the data were truncated at 150 eV to remove the influence of the previously defined hot population. A further thresholding was applied to only include points in the fit if their value was greater than 20% of the maximum (keeping points in the vicinity of the peak value). Using the polyfit routine in Matlab, a quadratic polynomial fit is performed on the natural log of the count rate data. The natural logarithm transforms Gaussian-like data into a parabola for input into the polyfit routine. This is a least squares problem of the form $Vp = y$, where V is a Vandermonde matrix constructed from the energy bin values, y is the logged count rate data and p is the least squares solution containing the polynomial coefficients. These coefficients determine the Gaussian parameters A_0 , A_1 , and A_2
- In polyfit weighted, an additional weight vector (w) is used, modifying the least squares problem to $Vp = yw$. Using the normalised root mean squared error (NRMSE) to quantify the closeness of Gaussian fit to the peak of the distribution, the best weight vector of form $w = y^i$ is found. Generally, $i = 4$ is found to work well. The weight vector essentially augments the count rate around the peak of the distribution such that a better fit at the peak would preferentially minimize the squared residuals
- The third method, nlinfit, is a nonlinear regression routine in Matlab which uses an iterative Levenberg-Marquardt least squares algorithm to estimate the Gaussian parameters that minimize the squared residuals between the counts data and the model, with initial values specified by the polyfit routine

The technique which showed the most stable results (i.e., without nonphysical values in the fitted Gaussian such as negative temperature) was used in determining the 1d temperature.

Fundamentally, heating is due to particles scattered from one region of velocity space into another region, increasing the volume in velocity space. Given that the 1d moment method restricts to a single Maxwellian population, an increase in the phase space density at higher energies would correspond to heating of that population. If the 1d derived Maxwellian fits well to the low energy spectra, then the magnetosheath population can be well described by a Maxwellian distribution. Furthermore, if the 1d plasma parameters are in close agreement with the 3days moments, then we can infer that the temperature and density moments of the entire distribution can be interpreted as Maxwellian plasma parameters of the dominant magnetosheath population. This is key for reliably determining the amount of heating caused by reconnection, rather than measuring the heating simply due to the additional presence of hotter magnetospheric electrons in the plasma.

After obtaining the observed heating ΔT_e for each event, we compared it with the theoretical value. The semi-empirical formula for electron bulk heating caused by magnetic reconnection is (Phan et al., 2013):

$$\Delta T_e = 0.017 m_i V_{\text{AL, in}}^2 = 0.017 \frac{B_{\text{L, in}}^2}{\mu_0 n_{\text{in}}}, \quad (9)$$

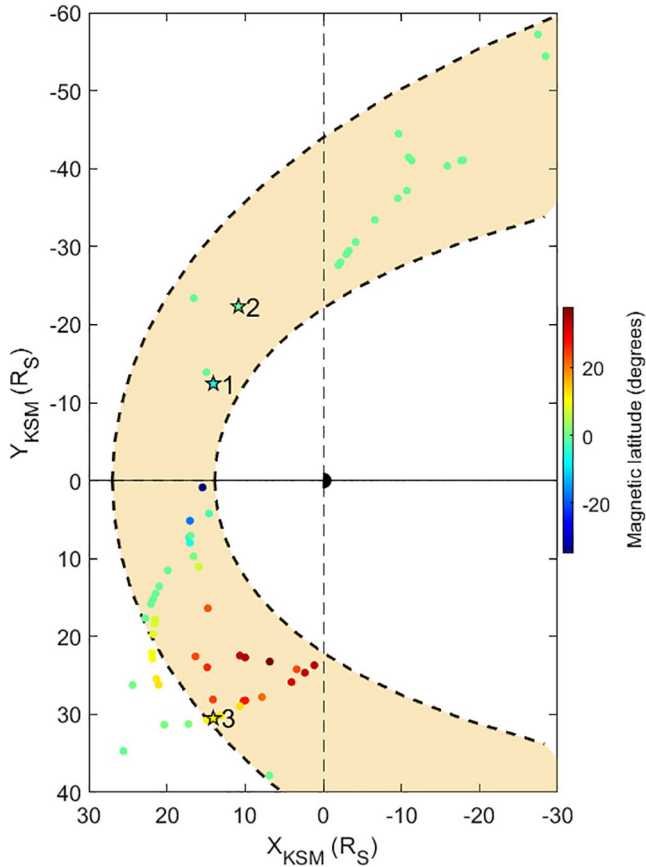


Figure 3. Positions of the 70 Cassini magnetopause crossings made between April 2005 to July 2007 projected onto the XY plane in Kronocentric Solar Magnetospheric (KSM) coordinates with determined full plasma β in both the magnetosheath and magnetosphere (Masters et al., 2012). The color of the markers indicates magnetic latitude (i.e., with respect to Saturn’s equatorial plane). The dashed black curves give extreme positions of Saturn’s magnetopause at standoff distance $14 R_S$ and $27 R_S$ based on model in Pilkington et al. (2015). The crossing positions shown as a star with labels 1, 2 and 3 correspond to the three case studies.

Three case studies of magnetopause crossings are presented to illustrate the characterization and varying amount of electron heating for each category of events. The locations of these exemplar crossings in the equatorial plane are shown as stars in Figure 3.

3.1. Case Study 1: Steady Magnetopause Crossing With Field Rotation and Substantial Electron Bulk Heating

Figure 4 shows an inbound magnetopause crossing by Cassini at low magnetic latitude (-6.44°) in the pre-noon sector (9:20 LT) at a radial distance of $19 R_S$ ($1 R_S = 60,268$ km is Saturn’s equatorial radius). The crossing duration was ~ 9.5 min. The magnetic shear across the MP was $\sim 93 \pm 4^\circ$, based on the dot product of the average fields in the intervals marked by the two pairs of dashed lines in Figure 4 either side of the MP. The eigenvalue ratio of the intermediate and minimum variance direction was $\lambda_2/\lambda_3 = 13$. As a rule of thumb, a well-defined boundary transition has $\lambda_2/\lambda_3 \approx 10$ (Sonnerup & Scheible, 1998). The ratio of the average normal component of the magnetic field compared with the average total field in the magnetopause is $B_N/B = 0.015 \pm 0.026$. This value is negligible within the error and indicates that the boundary may have been locally closed, forming a tangential discontinuity (TD). The magnetosheath and magnetospheric full

where $V_{AL,in}$ is the inflow Alfvén speed based on the inflow reconnecting field $B_{L,in}$ and number density n_{in} . Note that the expression is mass-independent. The constant 0.017 represents the fraction of inflow magnetic energy per proton-electron pair converted to heat. If a MP crossing lies in the “reconnection possible” regime in the $|\Delta\beta|$ -magnetic shear parameter space and the observed heating agrees with prediction within error then it is a good indicator that the spacecraft passed through an actual reconnection exhaust emanating from a reconnection site local to the spacecraft. Performing minimum variance analysis (MVA) (Sonnerup & Scheible, 1998) on the magnetic field data in the MP crossing interval yielded the maximum variance direction which determines the reconnecting field component (B_L). The energy stored in this field component is released during reconnection and converted to particle energy (see Equation 9). MVA also provides the minimum variance direction which is the normal component of the magnetic field B_N relative to the MP surface. We compared the single-sample MVA with the bootstrap MVA method. The main difference between the two methods was that the bootstrap method performed a large number of minimum variance calculations using bootstrap data samples of the set of magnetic vectors in the MP interval of interest (Sonnerup & Scheible, 1998). This produced a set of minimum variance eigenvectors and corresponding normal field components $\{B_N\}$. The average and standard deviation of this set were obtained and found to be close to the B_N value derived from the single-sample method which performs the minimum variance calculation once on the same interval of magnetic vectors, with analytical estimates of uncertainty typically of order 0.1 nT (Sonnerup & Scheible, 1998). The single-sample MVA was employed in this study. The obtained B_N value and its uncertainty are used to determine whether the MP boundary is “open” or “closed.”

Furthermore, the 70 events were put into three categories:

1. Steady transitions with field rotation (i.e., polarity change)
2. Turbulent transitions with field rotation
3. Transitions without significant field rotation (i.e., no polarity change)

Each event was also labeled by energization being 0 or 1, where energization of 1 means the heating values calculated from both the 1d and 3d methods for the cold population were >1.5 eV, with uncertainty typically of the order of 1 eV; otherwise the event was labeled energization of 0.

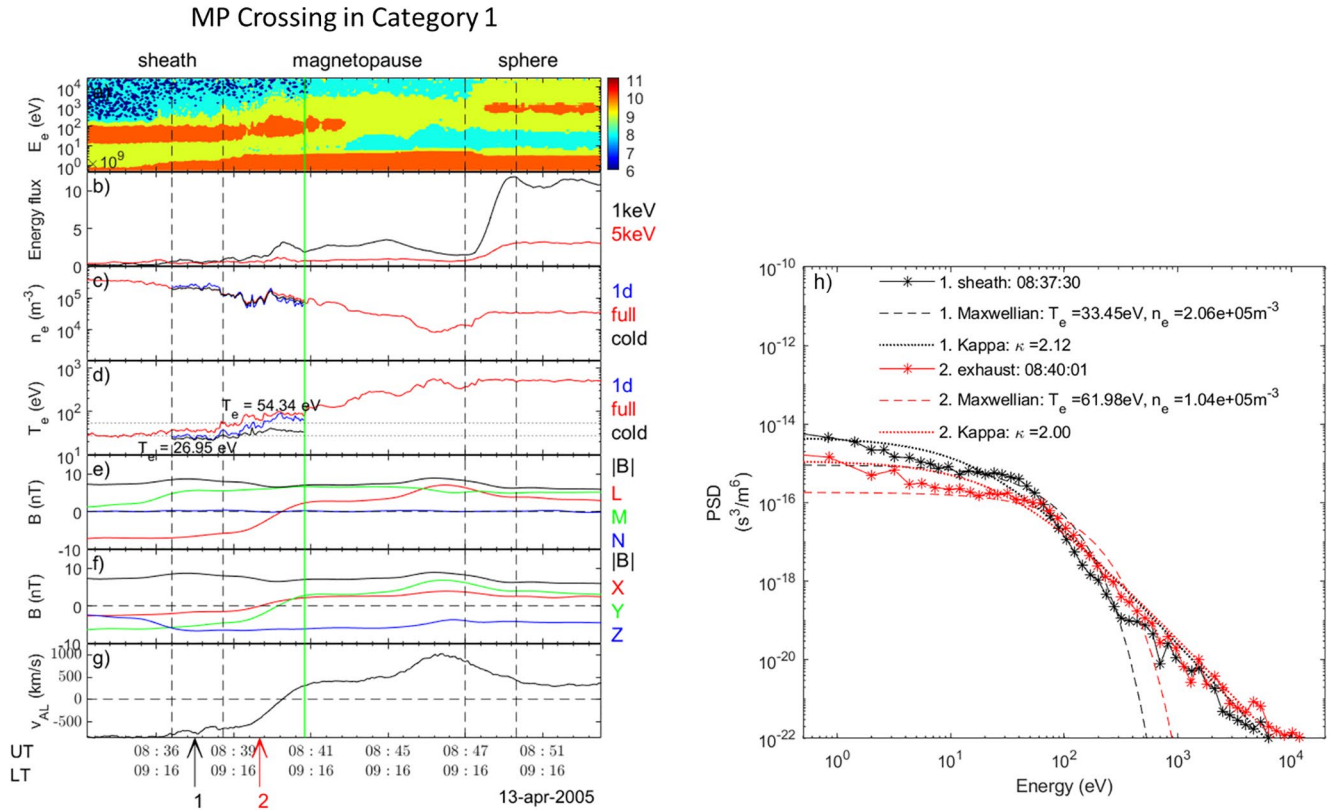


Figure 4. Exemplar magnetopause crossing with evidence of electron heating in category 1: Steady transition with field rotation. The panels are (a) Energy-time spectrogram of decimal logarithm of electron Differential Energy Flux (DEF) ($\text{eVs}^{-1}\text{m}^{-2}\text{ster}^{-1}\text{eV}^{-1}$) from ELS anode 5. The red band below ~ 5 eV is spacecraft photoelectrons. (b) DEF of 1 and 5 keV electrons. (c and d) Electron number density (m^{-3}) and temperature eV based on the 3d moment methods (full, cold) and 1d moment method (1d). (e) Magnetic field in minimum variance coordinates. (f) Magnetic field in KSM Coordinates. (g) Alfvén speed based on B_L and proton mass density. (h) Electron spectra in the magnetosheath (black) and in the MSBL (“exhaust”) (red) corrected for photoelectrons using the spacecraft potential, with overlaid Maxwellian distributions, and fitted Kappa distributions, using measured density and temperature moments (full) as the plasma parameters. Labels “1” and “2” under panel g point to the times of the cuts shown in panel h. The pairs of dashed black vertical lines immediately before and after the MP crossing denote the magnetosheath and magnetospheric intervals that define the boundary conditions of the magnetopause current layer. The green vertical line denotes the innermost location of the magnetosheath boundary layer for the computation of the average electron temperature in this region.

plasma β were ~ 1.0 and ~ 1.5 respectively, leading to a change of $\Delta\beta \approx 0.5$. The ion Alfvén speed based on the reconnecting field (B_L) was 386 ± 1 km/s. This event was an exemplar of category 1 due to the steady crossing conditions as shown by a well-defined red band of magnetosheath electrons in the spectrogram and clear transition in moments aligned with a polarity change in the B_L magnetic field component either side of the magnetopause. We describe the event from left to right going from the magnetosheath to the magnetosphere as we investigate the heating of the entering magnetosheath electrons.

Across the magnetosheath boundary layer (“exhaust”), the 1d temperature of the thermal population (containing most of the electrons) increased gradually, from $\sim 27 \pm 1$ eV (in the pristine magnetosheath) to $\sim 54 \pm 3$ eV in the exhaust (blue line in Figure 4d), where the uncertainty is the standard error of the mean temperature in each region. The temperature increased even further deeper within the magnetopause. Thus, the average amount of magnetosheath electron heating for this event was $\Delta T_{e,\text{obs}} = 27 \pm 2.6$ eV. The predicted heating due to reconnection using Equation 9 was $\Delta T_{e,\text{pred}} = 26.5 \pm 0.2$ eV which is in good agreement with the observation within uncertainty. The heating of the entering magnetosheath electrons is also evident in the electron energy-time spectrogram (Figure 4a), which shows an upward energy shift of the red band at the beginning of the exhaust. Since the 1D temperature depends on just the peak energy, a depletion in low energy electrons for example should not affect the temperature value and we can assume the measured heating is due to magnetosheath electrons being shifted to higher energy. Figure 4h shows representative electron PSD distributions in the magnetosheath (black) and in the exhaust (red);

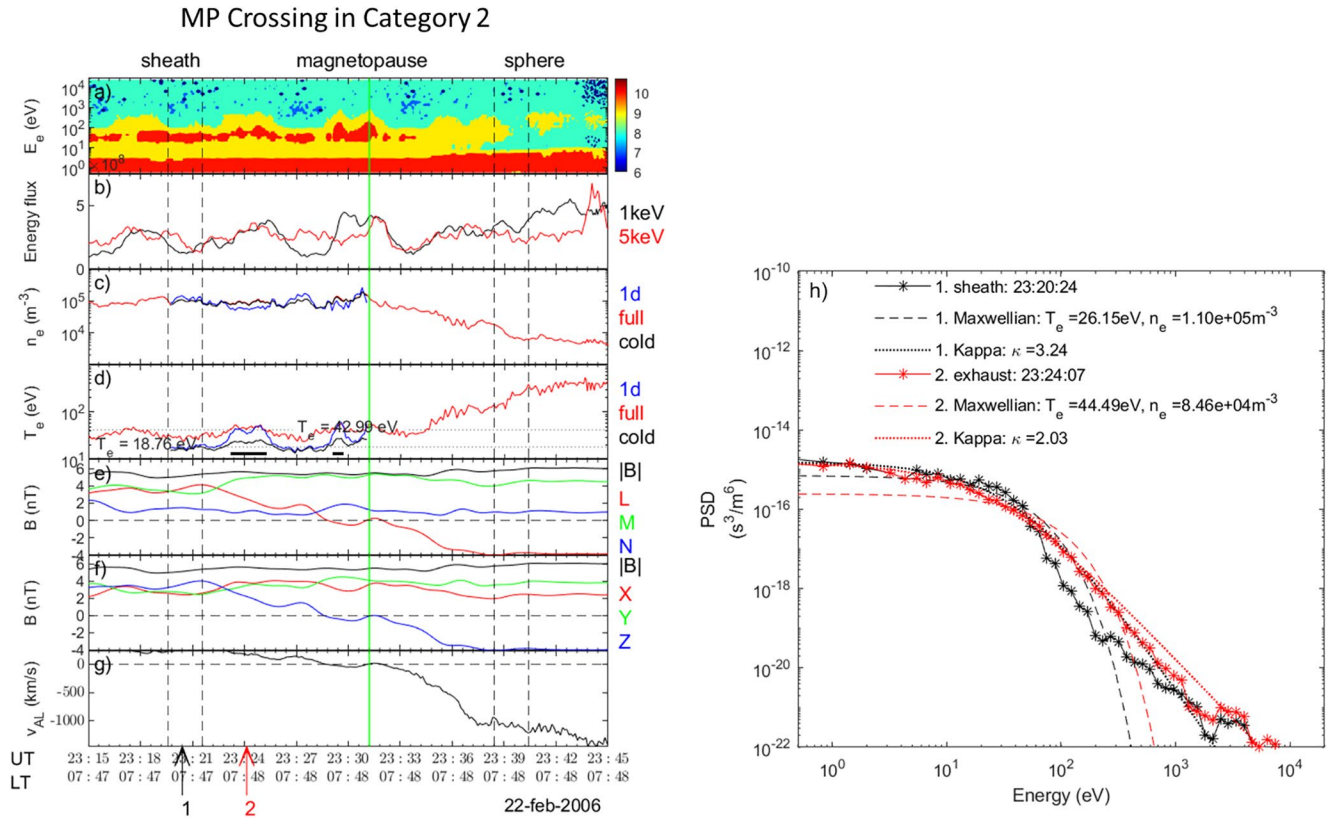


Figure 5. Exemplar magnetopause crossing with evidence of electron heating in category 2: Turbulent transition with field rotation. The format of the panels is identical to Figure 4.

3.2. Case Study 2: Turbulent Magnetopause Crossing With Field Rotation and Electron Bulk Heating

Figure 5 shows an inbound magnetopause crossing by Cassini at low magnetic latitude (-0.29°) near dawn (7:47 LT) at a range of $25 R_S$. The crossing duration was ~ 17 min. The magnetic shear across the magnetopause was $\sim 88.9 \pm 3^\circ$. The eigenvalue ratio of the intermediate and minimum variance magnetic field direction is $\lambda_2/\lambda_3 = 2.55$; this small value suggests a less reliable normal direction was obtained. The ratio of the average normal component of the magnetic field compared with the average total field in the MPCL is $B_N/B = 0.19 \pm 0.08$. This value is marginally non-zero, given the uncertainty, which suggests that the magnetopause could be magnetically open, forming a rotational discontinuity (RD). The magnetosheath and magnetospheric full plasma β were ~ 1.6 and ~ 0.5 respectively, leading to a change of $\Delta\beta \approx 1.1$. The ion Alfvén speed based on the reconnecting field (B_L) was 358 ± 2 km/s. This event is in category 2 due to more turbulent crossing conditions as seen in the patchy spectrogram with intermittent energization of the magnetosheath electrons and also breaks in the red band, likely due to mixing between magnetosheath and magnetospheric populations. However, there is still a clear polarity change in the B_L field either side of the MP.

In contrast to Case Study 1, the intermittent energization in this event caused an underestimation of the heating if we simply consider the average temperature in the entire exhaust (between the second dashed black line on the left and the green solid line in Figure 5). To mitigate this effect, the average temperature of only the heated electrons was used. This corresponded to time intervals of 23:23:24 to 23:25:12 UT and 23:28:48 to 23:29:24 UT (marked by horizontal bars in Figure 5d). Thus, the average amount of electron heating for this event was $\Delta T_{e,obs} = 24.2 \pm 1.5$ eV. The predicted heating due to reconnection was $\Delta T_{e,pred} = 22.8 \pm 0.3$ eV which is in good agreement with the observation within the uncertainty. Figure 5h shows that the exhaust PSD is clearly higher than the magnetosheath PSD around the 100 eV region, also indicative of heating.

In contrast to Case Study 1 and 2, the electron temperature did not increase in the exhaust and remained roughly constant until 15:55:12 UT when hot (>1 keV) magnetospheric electrons began to appear and density dropped monotonically (Figures 6b and 6c). The absence of bulk heating of entering magnetosheath electrons is also clear in the electron spectrogram, which shows essentially no variations across the MP. Similarly, Figure 6h shows that the electron spectra in the magnetosheath (black curve) and in the magnetosheath side of the magnetopause (red curve) were nearly identical. The average amount of bulk temperature change for this event was only $\Delta T_{e,obs} \approx 1.12 \pm 0.57$ eV. The predicted heating due to reconnection was $\Delta T_{e,pred} = 2.59 \pm 0.02$ eV. The discrepancy suggests that the conditions measured by the spacecraft may be quite different to those at any putative reconnection site. Furthermore, the small predicted value suggests that local conditions are not viable for reconnection. In such a case, in the absence of other evidence, one concludes that this is most likely a case of a closed magnetopause with no active reconnection. This conclusion would be consistent with hypothesis 1. A magnetic shear of $\sim 32^\circ$ and $\Delta\beta \approx 3.17$ places this event in the “reconnection suppressed” regime, consistent with hypothesis 2 that no significant energization was observed (nominal value of $\Delta T_{e,obs}$ is less than twice its uncertainty).

Of the three case studies, they all showed some level of both plasma depletion and magnetic field enhancement on approach to the MP through the magnetosheath (see Appendix A1). These signatures are suggestive of a plasma depletion layer (PDL) which could improve conditions for magnetic reconnection as it reduces plasma β near the magnetopause. PDLs usually form outside the dayside magnetopause as a result of compressed magnetic flux draping around the magnetospheric obstacle which generates a force that squeezes plasma out of the region resulting in a reduced density near the subsolar MP (e.g., Slavin et al., 1983). PDL reduces the plasma β due to stronger field strength and reduced number density which increases Alfvén speed at the MP (where reconnection may happen). If reconnection is efficient at the boundary, it can transport magnetic flux away fast enough so that there is less build-up of magnetic flux from the incoming solar wind toward the MP thus no PDL forms. PDLs appear to be a common occurrence at Saturn (Masters et al., 2014). Also seen in these events were relatively quasi-periodic anticorrelated changes in field strength and electron number density in the magnetosheath likely due to mirror mode waves (Cattaneo et al., 1998; Violante et al., 1995).

The key parameters responsible for the differences in bulk electron heating in these events are the change in plasma β ($\Delta\beta$) across the magnetopause, magnetic shear, and the Alfvén speed. The purpose of the statistical survey is to reveal whether there is a correlation between the agreement of observed and predicted heating and the parameters that play a role in the viability of reconnection at Saturn’s magnetopause, as detailed in Masters et al. (2012).

4. Results

A statistical overview of the 70 events is provided below. One event had unclear boundary crossing in both field and plasma parameters and was omitted from the analysis. We found 45 (66%), 12 (17%), and 12 (17%) events in categories 1, 2, and 3 respectively. Thirty nine (57%) events have an open MP based on the criteria of $B_N/B \geq 0.1$. Twenty eight (41%) events showed evidence of energization based on temperature change threshold of $\Delta T_e > 1.5$ eV after accounting for uncertainty. In all three methods of calculating heating, we find a few events with negative temperature change moving from pristine magnetosheath to magnetosheath edge of the MP, the largest being almost -5 eV based on the 1d temperatures. Note that the typical standard error of the mean temperature in each region is ~ 1 eV. There are also intrinsic errors at the source of measurements associated with the ELS sensor, such as Poisson counting statistical uncertainty and the assumption of isotropic distribution function as CAPS had limited angular coverage. Arridge et al. (2009) showed temperature uncertainty is less than 20% above a temperature of 10 eV which would lead to a temperature change between the two regions to be consistent with zero for these negative cases. On the other hand, if these cooling effects were real, it could be due to the presence of a PDL where more energetic magnetosheath electrons are expected to be preferentially evacuated along the direction of the piled-up magnetic field lines (Phan et al., 1994). One of the events on June 13, 2007 at $\sim 14:37$ UT showed signatures suggestive of this. Another possibility could be that the MP boundary is often not static due to varying pressures from external solar wind and internal plasma loading. The movement of the MP could change the thickness of the magnetosheath leading to expanded flux tubes which undergo adiabatic cooling. It may be possible

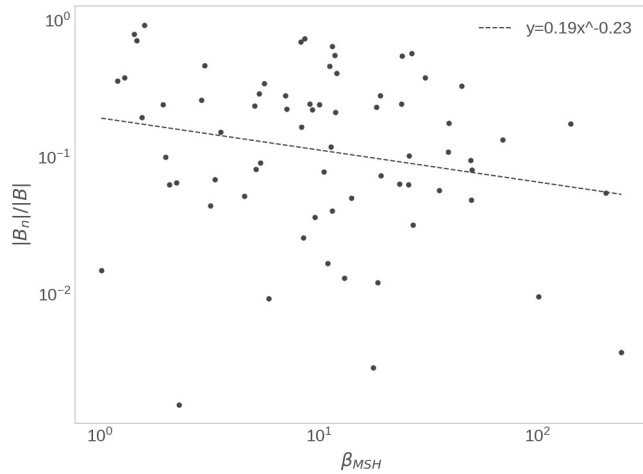


Figure 7. Evaluation of the relationship between the dimensionless reconnection rate B_n/B and magnetosheath plasma β with a power law fit (dashed line) to observations for the 70 magnetopause crossings at Saturn in this study.

that compressed flux tubes at the magnetopause could lead to adiabatic electron heating of similar magnitude, which could explain some of the electron heating events observed at locally closed magnetopause. These must remain speculative statements until future related analysis takes place. As discussed in case study 1, heating events at locally closed magnetopause may be magnetically connected to a remote reconnection site, which may be more probable as magnetic reconnection is common at Saturn’s magnetopause (Fuselier et al., 2020). In the current study, the electron heating measured at Saturn’s magnetopause was examined for evidence of magnetic reconnection. Fuselier et al. (2020) showed that it is possible to determine the incoming direction of the energized electrons detected by ELS using pitch angle data which could provide further evidence for energization caused by reconnection.

As discussed previously, the presence of PDL just external to the magnetopause reduces the plasma β . The dimensionless reconnection rate B_n/B is expected to increase with increasing ratio of magnetosheath to magnetospheric field strength (Sonnerup, 1974). Figure 7 shows the relationship between B_n/B with β_{MSH} and appears to qualitatively support that high B_n/B tend to occur in low- β cases, in correspondence with the results of Scurry et al. (1994) and DiBraccio et al. (2013). A power law of the form $y = ax^{-b}$ was fitted to the data giving parameters $a = 0.19 \pm 0.07$

and $b = 0.23 \pm 0.13$. The fit had an r^2 (or coefficient of determination) value of -0.158 which implies that the model fits worse than a horizontal line at the mean. The same conclusion was reached when considering a plot of B_n/B against B_{MSH}/B_{MSP} . More data points are needed to improve the uncertainty of the result.

The upstream solar wind Alfvén Mach number was estimated for each event to characterize the magnetosheath conditions. To first order approximation, the upstream solar wind magnetic field strength is a factor of 4 weaker than that of the downstream magnetosheath proper (Sulaiman et al., 2014, Figure 3). This allows upstream magnetic field strength (B_u) to be approximated from magnetosheath field measurements. The upstream dynamic pressure (P_{dyn}) can be approximated using the Kanani et al. (2010) MP model at the position of the crossing. Finally, the upstream Alfvén Mach number can be calculated via (Sulaiman et al., 2016)

$$M_A \equiv \frac{u}{v_A} = \frac{\sqrt{\mu_0 P_{dyn}}}{B_u} \quad (10)$$

For case studies 1, 2, and 3, M_A were 4.76, 5.56, and 14.71, respectively. Overall, the 70 events had a median upstream Alfvén Mach number of 12.37 with lower and upper quartiles at 7.9 and 17.0, respectively, which is only marginally lower than the typical median of 14 found at Saturn (Sulaiman et al., 2016). Analyzing more MP crossings would help improve the statistics, but this is left for future studies. Figure 8 shows that events with evidence of energization had a lower mean $M_A = 11.9$ than for those without energization with $M_A = 17.8$. After log transforming the two samples of M_A to make it approximately normally distributed, a t -test was performed for the means under a null hypothesis that two independent samples have identical means. A p -value of 0.03 was obtained implying the null hypothesis of equal means could be rejected at a significance level of 0.05. Masters (2015) explained that a larger solar wind M_A leads to less favorable magnetosheath conditions for magnetopause reconnection because it produces higher downstream plasma β and faster flows adjacent to the dayside magnetopause. A higher magnetosheath plasma β leads to greater $|\Delta\beta|$ across the magnetopause leading to greater diamagnetic drift suppression of reconnection (i.e.,

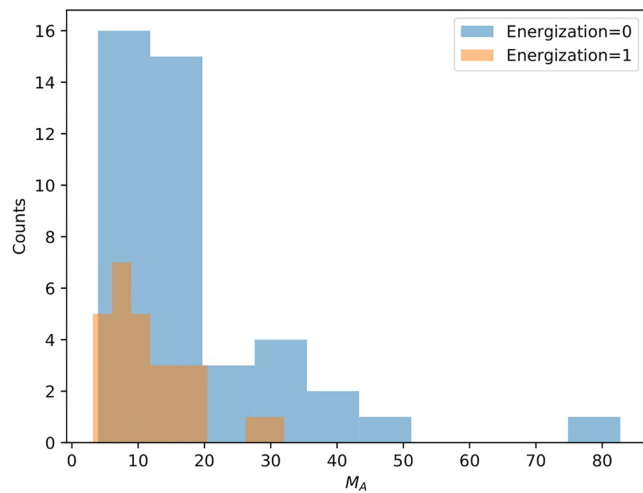


Figure 8. Histogram of the estimated upstream solar wind Alfvén Mach number for MP crossings with energization (orange) and without energization (blue).

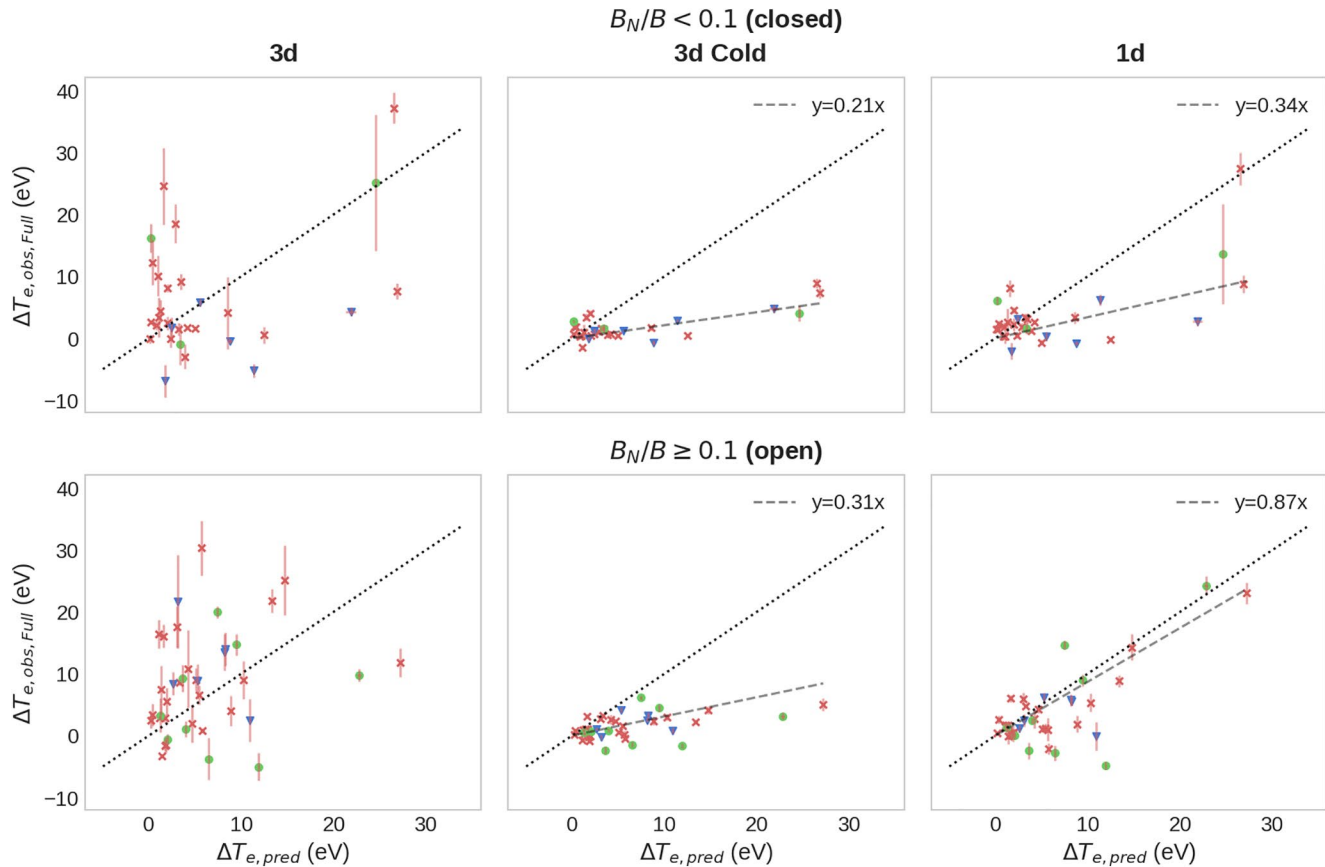


Figure 9. Observed against predicted bulk electron temperature change for all the crossings including results of error analysis. Left: Heating based on 3d moment method for full energy distribution. Middle: Heating based on 3d moment method for the cold energy distribution (<150 eV). Right: Heating based on 1d moment method for the peak of the energy distribution. Top panels represent locally “closed” boundary based on threshold $B_N/B < 0.1$. Bottom panels represent locally “open” boundary based on threshold $B_N/B \geq 0.1$. Red “x” markers: Steady transitions with field rotation (category 1). Green “o” markers: Turbulent transitions with field rotation (category 2). Blue “v” markers: Transitions without significant field rotation (category 3). The dotted line represents agreement between observed and predicted ΔT_e (assuming local reconnection). The error in $\Delta T_{e,obs}$ was calculated by adding in quadrature the uncertainty in the average magnetosheath and exhaust temperatures defined in the intervals between the pairs of vertical dashed lines as shown in the case studies (e.g., Figure 4).

onset restricted to near antiparallel magnetic fields) and greater flow shear suppression of reconnection at the magnetopause.

Plots of observed versus predicted electron temperature change for all 70 crossings using the three methods of temperature determination are shown in Figure 9. The events were subdivided into two groups based on their ratio of the normal component of the magnetic field (i.e., minimum variance component) compared with the average field strength in the magnetopause layer. A non-zero ratio within the error indicates an open magnetopause which could be an indicator of recent or ongoing reconnection local to the spacecraft. A ratio of $B_N/B = 0.1$ was used as a cutoff between “open” and “closed” boundary based on the assumption that, at a reconnecting magnetopause, we may assume that the field and particle velocities follow this relationship: $B_N/B = v_n/v_A = M_A$, where M_A is the Alfvén-Mach number (Sonnerup et al., 1981). At Earth, this ratio is roughly 0.1 (Sonnerup et al., 1981) but reconnection signatures at Saturn’s MP have been observed with $B_N/B = 0.04$ (McAndrews et al., 2008), indicating slower reconnection process than typically found at Earth. However, the average error for B_N/B was 0.03 based on analytical uncertainty estimates (Sonnerup & Scheible, 1998). Therefore, setting 0.1 as the threshold is a value which indicates that B_N/B is significantly non-zero (i.e., differs from zero by more than three standard error values). To assess how well the observed temperature changes match the semi-empirical predictions, a linear model is fitted to all 70 data points using weighted least squares method (from statsmodels module in Python) with intercept set to zero (not shown). The weight value is inversely proportional to the squared error. The reason for dropping the

intercept is due to Equation 9 which says that the presence of electron heating requires non-zero Alfvén speed, thus there should be no constant offset. Figure 9 shows the regression lines for the “3d cold” and “1d” methods. Note that negative temperature change events were not considered as they may be caused by different physical processes like PDL or adiabatic cooling (as discussed earlier).

For the 3d moment method based on the full observed energy distribution (left panels), the observations show little correlation to the prediction (assuming local reconnection). The regression performed on all data points gives a r^2 (or coefficient of determination) of 0.11 and a slope of 1.18 ± 0.42 . The r^2 value quantifies the proportion of the variance in the dependent variable ($\Delta T_{e,obs}$) that is predictable from the independent variables ($\Delta T_{e,pred}$). The low r^2 obtained clearly highlights the poor agreement between the observations and predictions. The slope being greater than unity indicates that using the temperature derived from the entire electron energy distribution tend to overestimate the temperature change due to the contamination from the hotter magnetospheric electrons. Thus, this method is unreliable in determining bulk temperature change due to reconnection for the magnetosheath electrons.

Considering the 3d moment method applied to the cold (<150 eV) part of the observed energy distribution (middle panels), the results show a much tighter spread with positive correlation and almost all observations are below predictions. The regression gives a slope of 0.21 ± 0.01 with r^2 of 0.49 for the closed case, and 0.31 ± 0.01 with r^2 of 0.60 for the open case. Note that this method produces systematically lower temperature changes as the summation in phase space density up to 150 eV implies no electrons at energies above 150 eV for the core population which is not the case. Thus, the slope is much smaller compared to the 1day method which is discussed next.

Electron heating calculated using the 1d method (right panels) show a clear positive correlation between the observation and prediction. The regression slope was 0.34 ± 0.02 with r^2 of 0.58 for the closed case, and 0.87 ± 0.03 with r^2 of 0.88 for the open case. The residual plot of the linear fit shows random distribution around zero. This result is suggestive of energization comparable to that associated with the reconnection process, albeit weaker than prediction on average. The sensitivity of the regression slope values for the “open” magnetopause case in the 1d method was found to be insignificantly affected at different B_N/B cutoffs of 0.04, 0.07 and 0.1. The slopes were 0.81, 0.85 and 0.87 respectively, with errors 0.03 for all three values, thus were consistent within their uncertainties. With regards to hypothesis 1 that an “open” magnetopause should show signs of heating close to prediction, we do see qualitatively a tendency of better agreement with prediction for the locally “open” boundary cases based on the threshold $B_N/B \geq 0.1$ for the minimum variance component of the magnetic field. For the case of locally “closed” boundary ($B_N/B < 0.1$), we observe qualitatively a cluster of points near $\Delta T_e \sim 0$, but also numerous cases of significant heating far from prediction. We find five cases where the observed heating exceeds prediction significantly (>3 eV) with typical uncertainties of the order of 1 eV. These results suggest that although the majority of events fit our hypothesis 1 within the uncertainty, the minority of events which do not, may be at a closed magnetopause, connected to a remote reconnection site.

The mass loading via magnetospheric sourced ions may reduce the reconnection rate and the fraction of energy conversion at Saturn’s magnetopause. Zhang et al. (2016) showed that heavy ion mass loading ($m_i > 8$) reduces the reconnection voltage at the dayside magnetopause. Fuselier et al. (2019) reported that ionospheric O^+ mass loading on the dayside magnetopause at Earth likely reduces the reconnection rate but reconnection is not suppressed. At Saturn, ions of magnetospheric origin can enter the magnetosheath either directly through the locally open magnetopause or as magnetospheric energetic neutral atoms (ENA) through the closed magnetopause, which are subsequently ionized by charge exchange with solar wind ions, becoming pickup ions. The heavy ions produce a lower Alfvén speed at the magnetopause that acts to reduce the reconnection rate (Cassak & Shay, 2007). As Equation 9 is a semi-empirical formula for bulk electron heating caused by reconnection at Earth’s magnetopause, it may need to be modified for Saturn’s magnetosphere. The middle and right panels of Figure 9 show that the predicted electron heating generally overestimates the observed electron heating and that the regression slopes are smaller than unity seem to support this scenario. The regression slope in the bottom right panel of Figure 9 suggests that the energy conversion factor in Equation 9 may be modified to 0.015 ± 0.001 at Saturn.

The Kolmogorov-Smirnov (KS) test was used to test whether the two independent samples of electron heating for open and closed MP are drawn from the same underlying continuous population. A two-sided test was used for the alternative hypothesis which states that the empirical cumulative distribution function (ECDF₁) of sample 1 is less or greater than the ECDF₂ of sample 2. The KS statistic is found from the maximum deviation between the ECDFs of the two samples. If the KS statistic is small or the p-value is high compared to a predefined significance level (e.g., $\alpha = 0.1$), then we cannot reject the null hypothesis that the two samples are from the same underlying distribution. The KS test assumes continuous distributions. We test the ratio $\Delta T_{e,obs,1d}/\Delta T_{e,pred}$ which acts as a quantitative measure of the closeness to the predicted heating; a value of one indicates perfect match. The mean and standard deviation of this ratio were 3.54 and 7.96 for closed MP, and 0.92 and 1.47 for open MP, respectively. The p-value obtained from this analysis was 0.56 when all events were considered. Neglecting the category 3 (blue “v”) events due to very low magnetic shear, yielded a p-value of 0.13. The latter result indicates that the null hypothesis could be rejected at a significance level of 0.13, indicating that the probability that the heating ratio distributions are identical is less than 13%. Performing a Welch’s *t*-test for the mean ratio of two independent samples, which does not assume equal population variance also yields a p-value of 0.13. This suggests that open MP heating values are clustered closer to their corresponding predicted values than for the case of the closed MP which supports hypothesis 1, at a significance level of 0.13.

A limitation of this study is the lack of temperature anisotropy measurements due to limited FOV of ELS. For reconnection, the heating is expected to be field aligned such that $\Delta T_{e\parallel} > \Delta T_{e\perp}$ (Phan et al., 2013). Thus, the temperature calculation under the isotropic assumption could be an overestimate or underestimate of the true bulk heating depending on whether ELS anode 5 was measuring electron flux parallel or perpendicular to the local magnetic field, or a combination of both at the time of observation. Based on the anisotropy of electron heating at Earth’s magnetopause found by Phan et al. (2013), the parallel heating can range between 1.27 to 6.25 times the perpendicular heating; depending on the magnetic shear across the magnetopause. Thus, the bulk heating given by $\Delta T_e = 1/3 \Delta T_{e\parallel} + 2/3 \Delta T_{e\perp}$ can range between $1.09 \Delta T_{e\perp}$ to $2.75 \Delta T_{e\perp}$, or $0.44 \Delta T_{e\parallel}$ to $0.86 \Delta T_{e\parallel}$, with the average of these ranges being $\Delta T_e \sim 2 \Delta T_{e\perp}$ or $\Delta T_e \sim 0.65 \Delta T_{e\parallel}$. If the perpendicular energy distribution was being measured by anode 5, the calculated electron temperature from the 3d and 1d moment methods may need to be doubled to get the true bulk heating value. Conversely, if the parallel temperature was being measured, the temperature moment may need to be multiplied by 0.65 to get the true bulk heating value. The effect of this on the results in Figure 9 would be multiplying the slope by either 2 or 0.65, but the reality is likely somewhere in between as it is unlikely that all the measurements were taken either parallel or perpendicular to the local field. The temperature anisotropy could be determined by using CAPS ELS pitch angle distribution spectrograms parallel and perpendicular to the local field. However, these measurements are seldom available together due to the limited field of view of CAPS.

Figure 10 shows the crossings in $|\Delta\beta|$ -magnetic shear parameter space. Magnetic shears are based on average fields either side of the MP. We find 83% of events with no energization were situated in the “reconnection suppressed” regime, and 43% of events with energization lie in the “reconnection possible” regime. This is based on the cutoff marked by the solid black line corresponding to a current sheet thickness of one ion inertial length ($L = d_i$, see Masters et al., 2012 for more detail). These results support hypothesis 2 to some extent.

Focusing on the “Energization = 1” panel (right), we find that there is a cluster of six category three events at the bottom of the plot with magnetic shear below 20° (i.e., near parallel magnetospheric and magnetosheath fields) and all reside in the “suppressed” regime despite observational evidence of heated electrons. These events are similar in behavior to “Reconnection Event 2” analyzed in McAndrews et al. (2008). Cassini is likely observing field lines connected to a distant X-line and measuring energized plasma originating from that reconnection site. This can be seen in the simplified diagram (Figure 1) of day side magnetopause reconnection, showing a possible spacecraft trajectory where the B-field orientation would stay relatively constant throughout the crossing. If we neglected these events, 59% of events with energization lie in the “reconnection possible” regime. Furthermore, the remaining events in the “Reconnection suppressed” region would lie very close to the $L = 2 d_i$ dashed line and may plausibly be included in the “reconnection possible” regime given the relatively large uncertainty in $\Delta\beta$ (see Figure

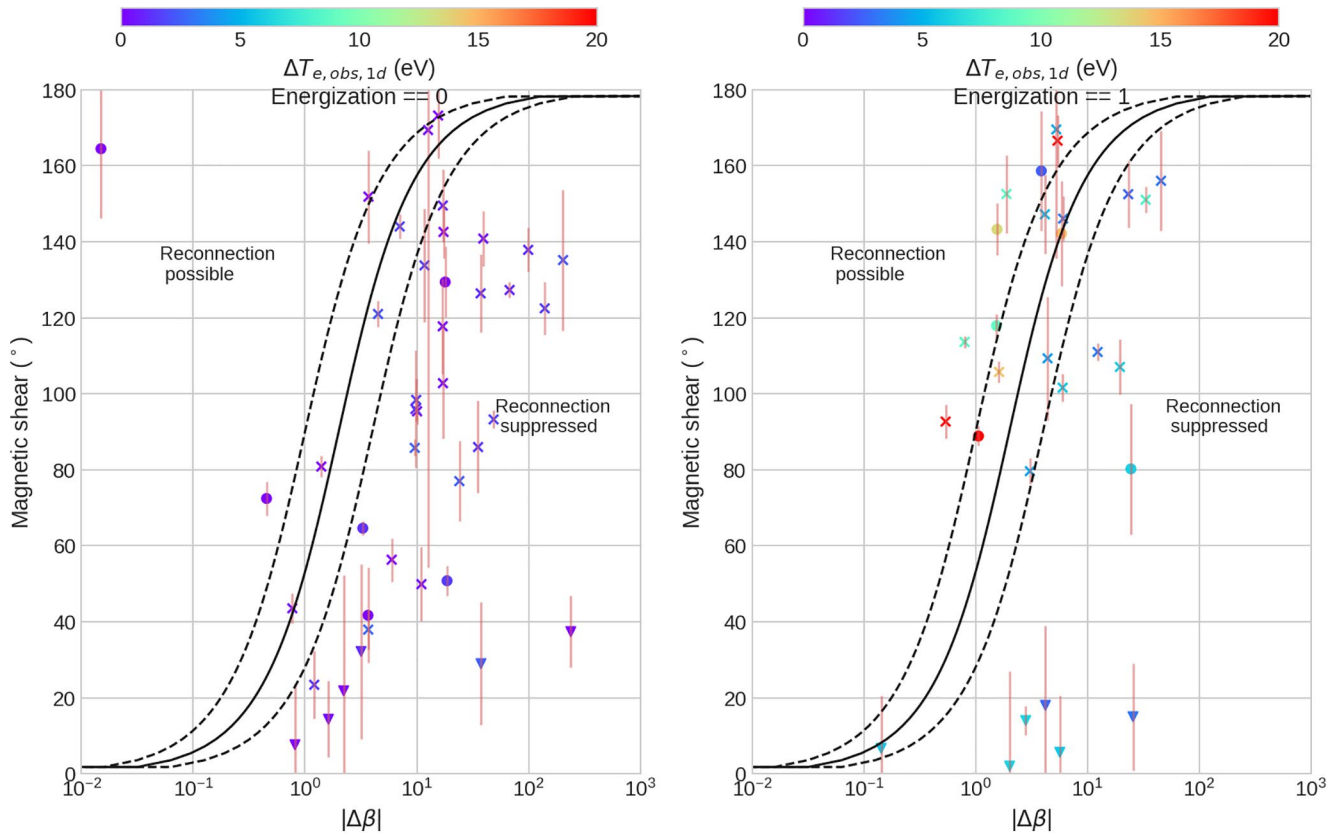


Figure 10. Assessment of diamagnetic suppression of reconnection using the 70 MP crossings, including error analysis. Color represents observed heating ΔT_e using the 1d moment method. The curves are calculated using Equation 1, where the solid line corresponds to a current sheet thickness $L = d_i$, and the dashed lines on the left and right of it correspond to $L = 0.5 d_i$ and $L = 2 d_i$, respectively. “x” markers: Steady transitions with field rotation. “o” markers: Turbulent transitions with field rotation. “v” markers: Transitions without significant field rotation. The error in $\Delta\beta$ can be found in Figure S2 in the supporting information of Masters et al. (2012). The error in magnetic shear was calculated using the general error propagation formula from the uncertainty in the average magnetic field either side of the magnetopause defined in the intervals between the pairs of vertical dashed lines as shown in the case studies (e.g., Figure 4).

S2 in supporting information of Masters et al., 2012). If we exclude the six “outliers” and use $L = 2 d_i$ as the threshold, we now find 68% of events with evidence of energization lie in the “reconnection possible” regime. Another interesting observation is that the rest of the events in the energization = 1 panel have magnetic shear above 80° suggestive of the high magnetic shear requirement. In addition, all the events to the left of the $L = d_i$ solid line contain the strongest heating observed at $\Delta T_e \geq 20$ eV including Case studies 1 and 2 (see Sections 3.1 and 3.2).

DiBraccio et al. (2013) tested the Swisdak et al. (2010) reconnection suppression condition at Mercury and found that the majority of the low- β events lie in the reconnection possible regime, including all crossings with reconnection rates $B_N/B \geq 0.25$. Sun et al. (2020) found that FTE showers (MP crossings with ≥ 10 flux ropes) at Mercury are most prevalent for high magnetic shear and low plasma β conditions. Both studies were consistent with the theoretical modeling of reconnection by Swisdak et al. (2010). A similar threshold applied to the 70 events in this study, however, found that large B_N/B were found either side of the suppression condition and for both energization and no energization cases. This suggests that B_N/B alone may not be a reliable indicator of magnetic reconnection occurring at Saturn, especially in cases where the IMF threads the magnetosheath such that the magnitude and direction is comparable to the field inside the magnetosphere, or the presence of Kelvin-Helmholtz waves, making the boundary identification unreliable with MVA. In addition, as the Saturnian system is much bigger than that of Mercury (by an order of ~ 100 times based on typical magnetopause standoff distance), it is possible to fly through flux tubes that were draping

around the magnetopause with large B_N/B as conditions were once favorable for reconnection but was no longer at the time of observation, and was perhaps magnetically conjugate to a reconnection site in which most of the energetic electrons have been transported away such that no heating was observed. For events without energization, most of the large B_N/B in fact occurred near the diamagnetic suppression condition suggesting conditions may have been favorable for reconnection in the past (see Appendix B1).

5. Conclusions

A statistical study of observed and theoretical electron bulk heating was performed at the magnetopause based on 70 magnetopause crossings detected by the Cassini spacecraft. Our hypotheses were: (1) Closed boundary should have no heating, whilst open boundary should have heating close to theoretical prediction (assuming local reconnection). We found that the 1d moment method for determining T_e supports this hypothesis the best, with strong correlation between observed and predicted ΔT_e for the case of open MP ($B_N/B \geq 0.1$), and a cluster of points near $\Delta T_e \sim 0$ for the case of closed MP. (2) Events with heating should reside in the “reconnection possible” regime and those without should lie in the “reconnection suppressed” regime in the $\Delta\beta$ -magnetic shear parameter space. We found 83% of events with no evidence of heating lie in the “reconnection suppressed” regime, whilst between 43% to 68% of events with evidence of heating lie in “reconnection possible” regime depending on the threshold used for current layer thickness. The results of this study reinforce the importance of plasma β and magnetic shear across the magnetopause on the viability of magnetic reconnection arising at observed locations.

One reason why some events do not fit our hypotheses is because we are assuming local conditions to be indicative of the putative reconnection site. However, the spacecraft could be quite distant from this site, and still magnetically connected to it. With a magnetosphere about 20 times larger than Earth's in absolute size, plasma accelerated by reconnection at Saturn may travel a large distance along field lines before reaching the spacecraft. Jasinski et al. (2014) showed an example of using the ion energy-pitch angle dispersion (observed by the CAPS Ion Mass Spectrometer) to estimate the distance to the reconnection site. Their cusp observation of electron energy distributions detected evidence for dayside magnetopause reconnection at a distance of up to $\sim 51 R_S$ from the reconnection site. Another important aspect is temporal variability in the near-magnetopause environment. The combination of spatial and temporal variability makes it possible to observe heated electrons with different ambient plasma and field conditions from the putative reconnection site, leading to discrepancies between theoretical predictions and observations. In addition to these factors, the events analyzed had relatively weak levels of heating, with only 6 out of 70 events with heating stronger than 10 eV, the strongest being around $\Delta T_e \approx 27$ eV. Some of these heating may be caused by mixing of magnetosphere and magnetosheath plasmas, as occurs at the MP. Finding events with higher magnetic field strength (e.g., when the magnetosphere is strongly compressed with a high magnetosheath field strength) would give faster inflow Alfvén speeds, and thus lead to stronger heating giving a reduced relative uncertainty for the observed heating. This would provide more data points at higher heating values and improve the statistics in comparing between the closed and open magnetopause. A more definitive conclusion on the hypotheses requires further analysis. We plan to analyze and augment the dataset further in future work utilizing recent magnetopause crossings lists (e.g., Jackman et al., 2019; Pilkington, et al., 2015), and taking the above aspects into consideration.

Appendix A: Case Studies: Signatures of Plasma Depletion Layer

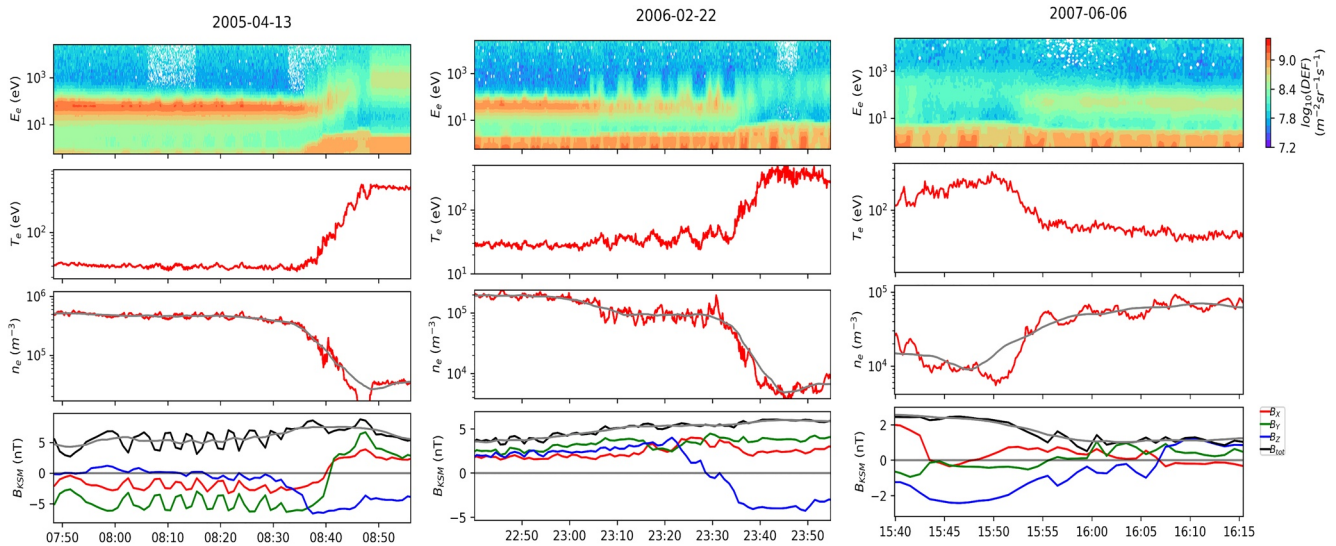


Figure A1. Cassini observations for the three case studies in this study, with signatures of increased field strength and decreased electron number density leading up to the magnetopause boundary. The gray solid lines are smoothed magnetic field strength and electron number density by taking the average in a 10 min window centered on each data point. All three events show some level of both density reduction and magnetic field enhancement on approach to the MP through the magnetosheath.

Appendix B: B_N/B and $\Delta\beta$ -Magnetic Shear

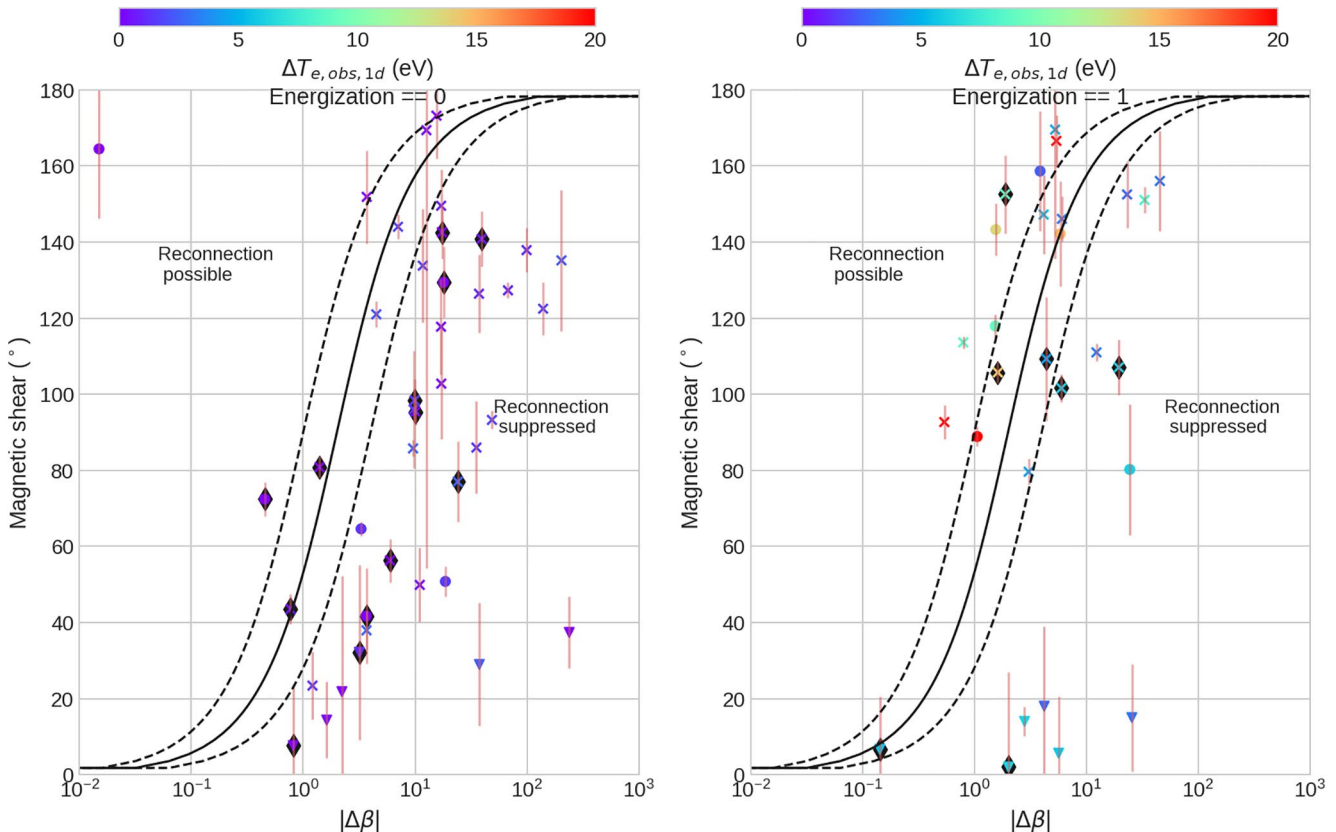


Figure B1. Events in magnetic shear- $\Delta\beta$ parameter space separated by Swisdak et al. (2010) diamagnetic suppression condition for reconnection. Black diamonds are crossings with $B_N/B \geq 0.25$.

Data Availability Statement

The magnetopause crossings of the Cassini spacecraft used in this study were identified and characterized by Masters et al. (2012) using the Cassini MAG, ELS, MIMI, and IMS data available from the Planetary Data System (<http://pds.nasa.gov/>).

Acknowledgments

IC was supported by a UK STFC studentship hosted by the UCL center for Doctoral Training in Data Intensive Science. NA and PG were supported by UK STFC Consolidated Grant number ST/S000240/1 (UCL/MSSL-Physics and Astronomy Solar System). AM was supported by a Royal Society University Research Fellowship. The authors wish to thank R.J. Wilson for invaluable discussions and useful comments about this work, and to thank G. Lewis for help with CAPS-ELS data.

References

- Arridge, C. S., Gilbert, L. K., Lewis, G. R., Sittler, E. C., Jones, G. H., Kataria, D. O., et al. (2009). The effect of spacecraft radiation sources on electron moments from the Cassini CAPS electron spectrometer. *Planetary and Space Science*, *57*(7), 854–869. <https://doi.org/10.1016/j.pss.2009.02.011>
- Baines, K. H., Flasar, F. M., Krupp, N., & Stallard, T. (Eds.), (2018). *Saturn in the 21st century*. Cambridge University Press. <https://doi.org/10.1017/9781316227220>
- Coates, P. A., & Shay, M. A. (2007). Scaling of asymmetric magnetic reconnection: General theory and collisional simulations. *Physics of Plasmas*, *14*(10), 102114. <https://doi.org/10.1063/1.2795630>
- DiBaccio, G. A., Slavin, J. A., Boardsen, S. A., Anderson, B. J., Korth, H., Zurbuchen, T. H., et al. (2013). MESSENGER observations of magnetopause structure and dynamics at Mercury. *Journal of Geophysical Research: Space Physics*, *118*(3), 997–1008. <https://doi.org/10.1002/jgra.50123>
- Dougherty, M. K., Kellock, S., Southwood, D. J., Balogh, A., Smith, E. J., Tsurutani, B. T., et al. (2004). The Cassini magnetic field investigation. *Space Science Reviews*, *114*(1–4), 331–383. <https://doi.org/10.1007/s11214-004-1432-2>
- Fuselier, S. A., Petrinec, S. M., Sawyer, R. P., Mukherjee, J., & Masters, A. (2020). Suppression of magnetic reconnection at Saturn's low-latitude magnetopause. *Journal of Geophysical Research: Space Physics*, *125*(5). <https://doi.org/10.1029/2020ja027895>
- Fuselier, S. A., Trattner, K. J., Petrinec, S. M., Denton, M. H., Toledo-Redondo, S., André, M., et al. (2019). Mass loading of the Earth's dayside magnetopause boundary layer and its effect on magnetic reconnection. *Geophysical Research Letters*, *46*(12), 6204–6213. <https://doi.org/10.1029/2019gl082384>
- Jackman, C. M., Thomsen, M. F., & Dougherty, M. K. (2019). Survey of Saturn's magnetopause and bow shock positions over the entire Cassini mission: Boundary statistical properties and exploration of associated upstream conditions. *Journal of Geophysical Research: Space Physics*, *124*, 8865. <https://doi.org/10.1029/2019ja026628>
- Jasinski, J. M., Arridge, C. S., Lamy, L., Leisner, J. S., Thomsen, M. F., Mitchell, D. G., et al. (2014). Cusp observation at Saturn's high-latitude magnetosphere by the Cassini spacecraft. *Geophysical Research Letters*, *41*(5), 1382–1388. <https://doi.org/10.1002/2014GL059319>
- Kanani, S. J., Arridge, C. S., Jones, G. H., Fazakerley, A. N., McAndrews, H. J., Sergis, N., et al. (2010). A new form of Saturn's magnetopause using a dynamic pressure balance model, based on in situ, multi-instrument Cassini measurements. *Journal of Geophysical Research*, *115*(A6). <https://doi.org/10.1029/2009ja014262>
- Kane, M., Mitchell, D. G., Carbary, J. F., Dialynas, K., Hill, M. E., & Krimigis, S. M. (2020). Convection in the Magnetosphere of Saturn during the cassini mission derived from MIMI INCA and CHEMS measurements. *Journal of Geophysical Research: Space Physics*, *125*(2), 1–21. <https://doi.org/10.1029/2019ja027534>
- Lewis, G. R., André, N., Arridge, C. S., Coates, A. J., Gilbert, L. K., Linder, D. R., & Rymer, A. M. (2008). Derivation of density and temperature from the Cassini-Huygens CAPS electron spectrometer. *Planetary and Space Science*, *56*, 901–912. <https://doi.org/10.1016/j.pss.2007.12.017>
- Masters, A. (2015). Magnetic reconnection at Neptune's magnetopause. *Journal of Geophysical Research: Space Physics*, *120*(1), 479–493. <https://doi.org/10.1002/2014ja020744>
- Masters, A. (2018). A more viscous-like solar wind interaction with all the giant planets. *Geophysical Research Letters*, *45*(15), 7320–7329. <https://doi.org/10.1029/2018GL078416>
- Masters, A., Eastwood, J. P., Swisdak, M., Thomsen, M. F., Russell, C. T., Sergis, N., et al. (2012). The importance of plasma β conditions for magnetic reconnection at Saturn's magnetopause. *Geophysical Research Letters*, *39*(8). <https://doi.org/10.1029/2012GL051372>
- McAndrews, H. J., Owen, C. J., Thomsen, M. F., Lavraud, B., Coates, A. J., Dougherty, M. K., & Young, D. T. (2008). Evidence for reconnection at Saturn's magnetopause. *Journal of Geophysical Research*, *113*. <https://doi.org/10.1029/2007JA012581>
- Oieroset, M., Phan, T. D., Fujimoto, M., Lin, R. P., & Lepping, R. P. (2001). In situ detection of collisionless reconnection in the Earth's magnetotail. *Nature*, *412*(6845), 414–417. <https://doi.org/10.1038/35086520>
- Phan, T. D., Gosling, J. T., Paschmann, G., Pasma, C., Drake, J. F., Oieroset, M., et al. (2010). The dependence of magnetic reconnection on plasma β and magnetic shear: Evidence from solar wind observations. *Acta Pathologica Japonica*, *719*, L199–L203. <https://doi.org/10.1088/2041-8205/719/2/L199>
- Phan, T. D., Shay, M. A., Gosling, J. T., Fujimoto, M., Drake, J. F., Paschmann, G., et al. (2013). Electron bulk heating in magnetic reconnection at Earth's magnetopause: Dependence on the inflow Alfvén speed and magnetic shear. *Geophysical Research Letters*, *40*(17), 4475–4480. <https://doi.org/10.1002/grl.50917>
- Pierrard, V., & Lazar, M. (2010). Kappa Distributions: Theory and Applications in Space Plasmas. *Solar Physics*, *267*(1), 153–174. <https://doi.org/10.1007/s11207-010-9640-2>
- Pilkington, N. M., Achilleos, N., Arridge, C. S., Guio, P., Masters, A., Ray, L. C., et al. (2015). Internally driven large-scale changes in the size of Saturn's magnetosphere. *Journal of Geophysical Research: Space Physics*, *120*(9), 7289–7306. <https://doi.org/10.1002/2015JA021290>
- Pilkington, N. M., Achilleos, N., Arridge, C. S., Masters, A., Sergis, N., Coates, A. J., & Dougherty, M. K. (2014). Polar confinement of Saturn's magnetosphere revealed by in situ Cassini observations. *Journal of Geophysical Research: Space Physics*, *119*(4), 2858–2875. <https://doi.org/10.1002/2014JA019774>
- Phan, T.-D., Paschmann, G., Baumjohann, W., Sckopke, N., & Lühr, H. (1994). The magnetosheath region adjacent to the dayside magnetopause: AMPTE/IRM observations. *Journal of Geophysical Research*, *99*(A1), 121. <https://doi.org/10.1029/93ja02444>
- Scurry, L., Russell, C. T., & Gosling, J. T. (1994). Geomagnetic activity and the beta dependence of the dayside reconnection rate. *Journal of Geophysical Research*, *99*(A8), 14811. <https://doi.org/10.1029/94ja00794>
- Sonnerup, B., & Scheible, M. (1998). Minimum and maximum variance analysis. In *Analysis methods for multi-spacecraft data* (Vol. 001, pp. 185–220).
- Sonnerup, B. U. Ö. (1974). Magnetopause reconnection rate. *Journal of Geophysical Research*, *79*(10), 1546–1549. <https://doi.org/10.1029/ja079i010p01546>

- Sonnerup, B. U. Ö., Paschmann, G., Papamastorakis, I., Scokopke, N., Haerendel, G., Bame, S. J., et al. (1981). Evidence for magnetic field reconnection at the Earth's magnetopause. *Journal of Geophysical Research*, *86*(A12), 10049. <https://doi.org/10.1029/ja086ia12p10049>
- Sulaiman, A. H., Masters, A., & Dougherty, M. K. (2016). Characterization of Saturn's bow shock: Magnetic field observations of quasi-perpendicular shocks. *Journal of Geophysical Research: Space Physics*, *121*(5), 4425–4434. <https://doi.org/10.1002/2016ja022449>
- Sulaiman, A. H., Masters, A., Dougherty, M. K., & Jia, X. (2014). The magnetic structure of Saturn's magnetosheath. *Journal of Geophysical Research: Space Physics*, *119*(7), 5651–5661. <https://doi.org/10.1002/2014ja020019>
- Sun, W. J., Slavin, J. A., Smith, A. W., Dewey, R. M., Poh, G. K., Jia, X., et al. (2020). Flux transfer event showers at Mercury: Dependence on plasma β and magnetic shear and their contribution to the Dungey cycle. *Geophysical Research Letters*, *47*(21). <https://doi.org/10.1029/2020gl089784>
- Swisdak, M., Opher, M., Drake, J. F., & Alouani Bibi, F. (2010). The vector direction of the interstellar magnetic field outside the heliosphere. *Acta Pathologica Japonica*, *710*(2), 1769–1775. <https://doi.org/10.1088/0004-637X/710/2/1769>
- Swisdak, M., Rogers, B. N., Drake, J. F., & Shay, M. A. (2003). Diamagnetic suppression of component magnetic reconnection at the magnetopause. *Journal of Geophysical Research*, *108*(A5). <https://doi.org/10.1029/2002JA009726>
- Thomsen, M. F., Reisenfeld, D. B., Delapp, D. M., Tokar, R. L., Young, D. T., Crary, F. J., et al. (2010). Survey of ion plasma parameters in Saturn's magnetosphere. *Journal of Geophysical Research*, *115*(10). <https://doi.org/10.1029/2010JA015267>
- Yamada, M., Kulsrud, R., & Ji, H. (2010). Magnetic reconnection. *Reviews of Modern Physics*, *82*(1), 603–664. <https://doi.org/10.1103/RevModPhys.82.603>
- Young, D. T., Berthelier, J. J., Blanc, M., Burch, J. L., Bolton, S., Coates, A. J., et al. (2005). Composition and Dynamics of Plasma in Saturn's Magnetosphere. *Science*, *307*(5713), 1262–1266. <https://doi.org/10.1126/science.1106151>
- Young, D. T., Berthelier, J. J., Blanc, M., Burch, J. L., Coates, A. J., Goldstein, R., et al. (2004). Cassini plasma spectrometer investigation. *Space Science Reviews*, *114*(1–4), 1–112. <https://doi.org/10.1007/s11214-004-1406-4>
- Zhang, B., Brambles, O. J., Wiltberger, M., Lotko, W., Ouellette, J. E., & Lyon, J. G. (2016). How does mass loading impact local versus global control on dayside reconnection? *Geophysical Research Letters*, *43*(5), 1837–1844. <https://doi.org/10.1002/2016gl068005>